Vincenzo Di Capua

Tutor: Prof. Pasquale Arpaia

XXXIV Cycle - III year presentation

Real-time magnetic measurement system for synchrotrons control

My background

Graduation:

- Bachelor degree cum laude in Electronic Engineering from the University of Naples “Federico II” on
  October 5, 2016.
  Thesis: "Triaxial acceleration measurement with ARM STM32 microcontroller and MEMS INMO LSM6DS0 sensor on bus I2C”.

- Master degree cum laude in Electronic Engineering from the University of Naples “Federico II” on September 27, 2018.
  Thesis: "Development and Implementation of a Real-Time Magnetic Measurement Monitoring System for CERN B-Train”.

Fellowship:

- PhD Student of XXXIV cycle in Information Technology and Electrical Engineering (ITEE).
  Theme: “Real-time measurement and prediction of the magnetic field in particle accelerators”
- Doctoral student contract at the European Organization for Nuclear Research (CERN)

Collaborations

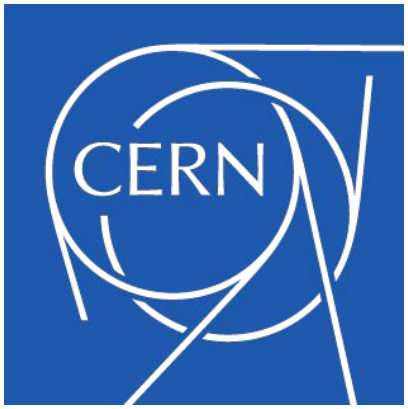

IMPALAB

Credit summary

	Credits year 1								Credits year 2								Credits year 3									
	Estimated	1 bimonth	2 bimonth	3 bimonth	4 bimonth	5 bimonth	6 bimonth	Summary	Estimated	1 bimonth	2 bimonth	3 bimonth	4 bimonth	5 bimonth	6 bimonth	Summary	Estimated	1 bimonth	2 bimonth	3 bimonth	4 bimonth	5 bimonth	6 bimonth	Summary	Total	Check
Modules	10	0	0,4	0	8,2	0	0,4	**9**	10	0	0	0	0	0	10	**10**	21	4	0	6	5	3	5	**23**	**42**	**30-70**
Seminars	4	0	0,5	0	0	0	1,5	**2**	10	0,5	0,5	0,5	0,5	0,5	6,5	**9**	5	0,5	0,5	0,5	2	0,5	2	**6**	**17**	**10-30**
Research	52	9	9	9	9	9	9	**54**	50	9	9	9	9	9	9	**54**	40	7	7	7	7	7	5	**40**	**148**	**80-140**
	66	9	9,9	9	17,2	9	10,9	**65**	70	9,5	9,5	9,5	9,5	9,5	25,5	**73**	66	11,5	7,5	13,5	14	10,5	12	**69**	**207**	**180**

- Gregory Clement, “Linux kernel driver development (Bootlin)”, (10 CFU)
- Multiple Speakers (CERN), “Finding happiness in patent information databases”, (1 CFU)
- Elias Fernandez-Combarro Alvarez (CERN), “A practical introduction to quantum computing: from qubits to quantum machine learning and beyond”, (4 CFU)
- Stephane Deghaye, “Controlling the CERN Accelerator Complex”,(3 CFU)

Content

- Context
- Problem
- Relevance
- Research Topics
- Approach
- Hardware used
- Development
- Analog interface
- Integration process
- Field simulation
- Field prediction
- Tool for diagnostic and characterization
- System DC characterization
- System Dynamic characterization
- Drift free integrators and data fusion
- Side activities
- Production

Context

- **Synchrotrons:**
  Synchrotrons are a specific branch of particle accelerator, in particular, they are circular machines. The main components of a synchrotron are the Radio Frequency (RF) cavities and the magnets and they are disposed in a circular geometry called ring

➢ **RF cavities:** are used to accelerate (or decelerate) the charged particles providing energy to the beam thanks to an electromagnetic field.

➢ **Magnets:** are used to steer the beam and keep it tight during its orbit.

Lorentz law: $$\boldsymbol{F}(t) = q(\boldsymbol{E}(t) + \boldsymbol{v}(t) \times \boldsymbol{B}(t))$$

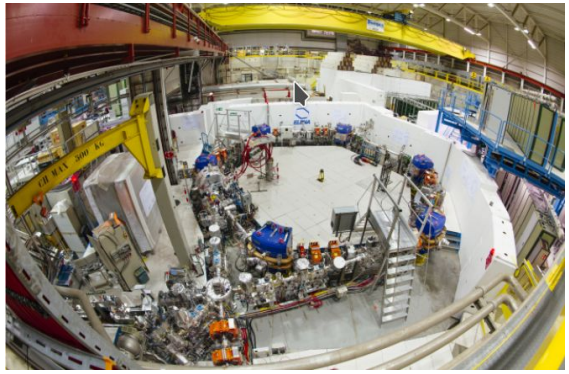

Extra low Energy Antiproton (ELENA) decelerator installation.

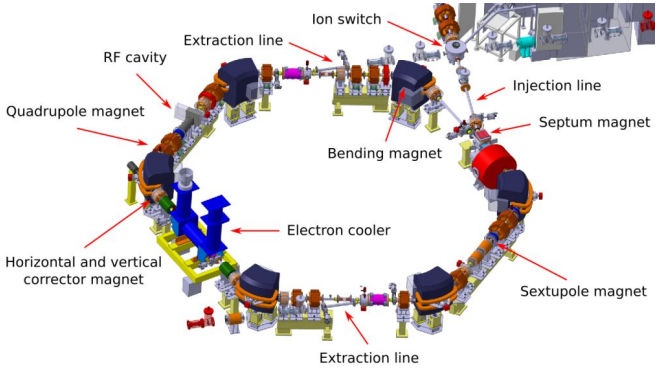

ELENA Layout.

Context

- **CERN Synchrotrons:**
  The accelerator complex at CERN, includes eight accelerators (machines) that accelerate particles in order to increase their energy. Each machine in the chain increases the energy of the particles by a factor typically around 20 limited by non-linearities, before delivering them to the next more powerful accelerator or to experiments. There are four main experiments in theLHC (CMS, ATLAS, LHCb and ALICE) and dozen of smaller experiments;
  each of them studies particle collisions from a different aspect and with different technologies.

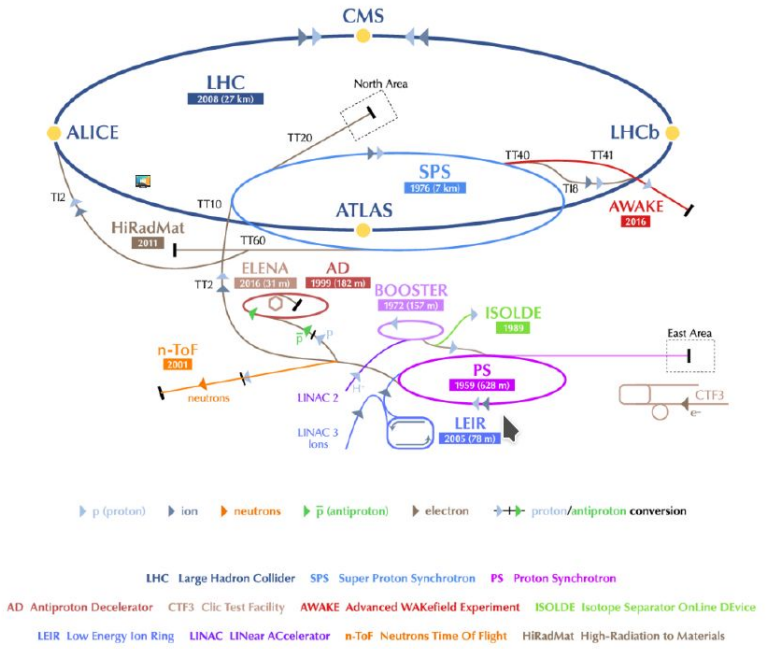

CERN Accelerator complex.

Problem

- The precise knowledge of the magnetic field produced by dipole magnets is critical for machine operations and real-time measurement systems are required, to acquire the magnetic field and feed it back to various subsystems in charge of the control of the magnets, especially in the case of iron-dominated electromagnets with strong non-linear effects such as eddy currents, hysteresis and saturation.

- Magnetic measurements in magnets for particle accelerators are performed in two scenarios: offline, after the magnet manufacturing and before the magnet installation as part of the quality assurance process. Online and in real-time during the machine operations, as necessary feedback for other accelerator's subsystems.

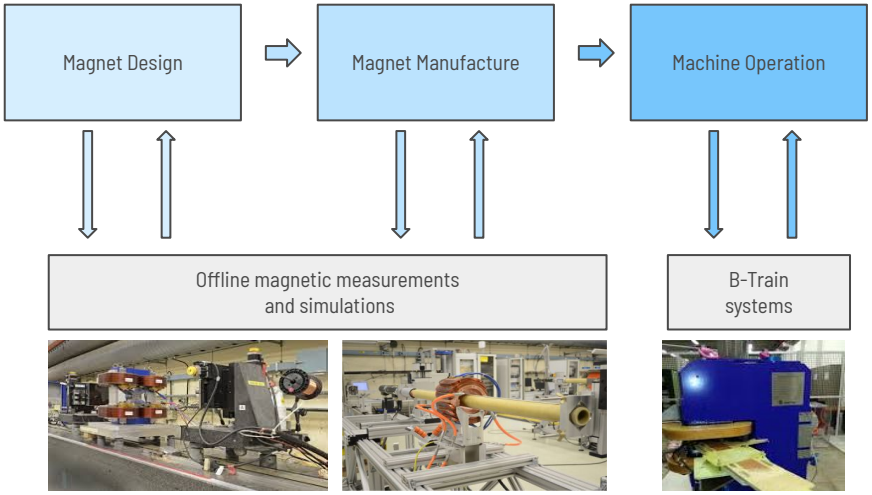

Role of measurements and simulations in magnetic design, manufacture and operations

Problem

- The Synchrotrons at CERN employ systems so-called B-train for determining the dipole field in real-time. The name derives from the discrete positive and negative pulse trains used to distribute incrementally the measured field in out-of-date systems, developed as far back as the 1950s.

- The out-of-date digital transmission (dating from the early 1960s) uses two coaxial cables to distribute 24 V pulses which indicate a ± 0.1 Gauss increase or decrease of magnetic field, i.e. up and down pulses. These pulses are distributed from the reference magnet to several client applications.

- Currently, all six B-train systems in operation are being upgraded in the frame of a long-term complex-wide consolidation project.

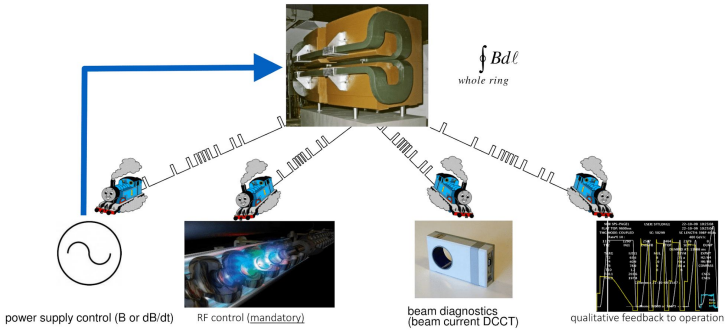

Relevance

- The precise knowledge of the magnetic field produced by dipole magnets is critical not only for the operation of a synchrotron but also in fusion engineering applications, where field measurements are used for diagnostic monitoring of the magnetic field interacting with the plasma.

- Many are the sensors that could be used for magnetic measurements, each kind of sensor has its specific field of application and its peculiarity. For this reason, they have to be carefully chosen and the data coming out need appropriate manipulation to be used.

- Typically custom hardware and software are needed to elaborate the data and to provide a real-time accurate measure of the magnetic field.

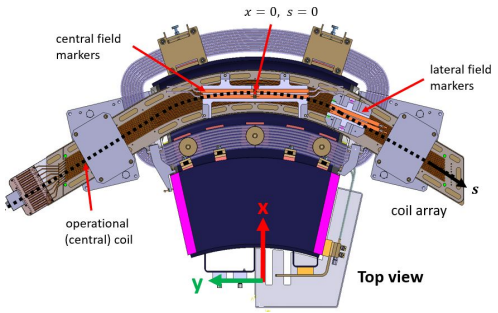

Sensors positioning in the ELENA reference magnet

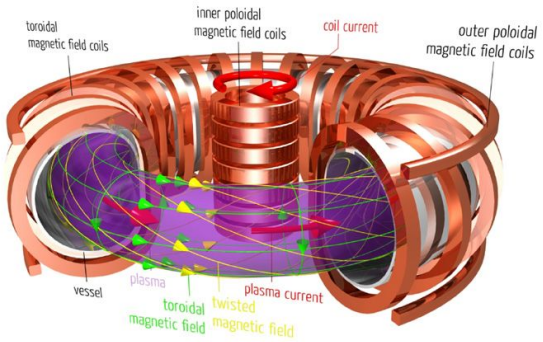

ITER magnets

Research topics

- 5 aspects were analyzed and treated:
  - The development and the implementation of a real-time measurement system starting from the system requirements defined by the final users (i.e. low level radio frequency, power converters and machine operators).
  - The development of a necessary tool to monitor in real-time the magnetic field provided by the seven installed systems over the optic-fiber.
  - The DC and dynamic performance evaluation of the presented system.
  - Exploitation of the possibility to use neural networks to predict the magnetic field, and all its non linearity such as eddy currents and hysteresis inside magnets for particle accelerators.
  - Drift-free integrator using kalman filtering for magnetic measurements.
- Side activity: A metabolic predictor for patient suffering from DIA1.
- Side activity: Vascularization quality assessment for laparoscopic surgery.

Approach

- Measurements are carried out in a suitable reference magnet, which is ideally installed in a dedicated room outside of the synchrotron and is powered in series with the ring magnets.

- A combination of two primary sensors:
  - An induction coil to measure the rate of change of the field according to Faraday's law.
  - A so-called field marker to provide the necessary integration constant B_M.

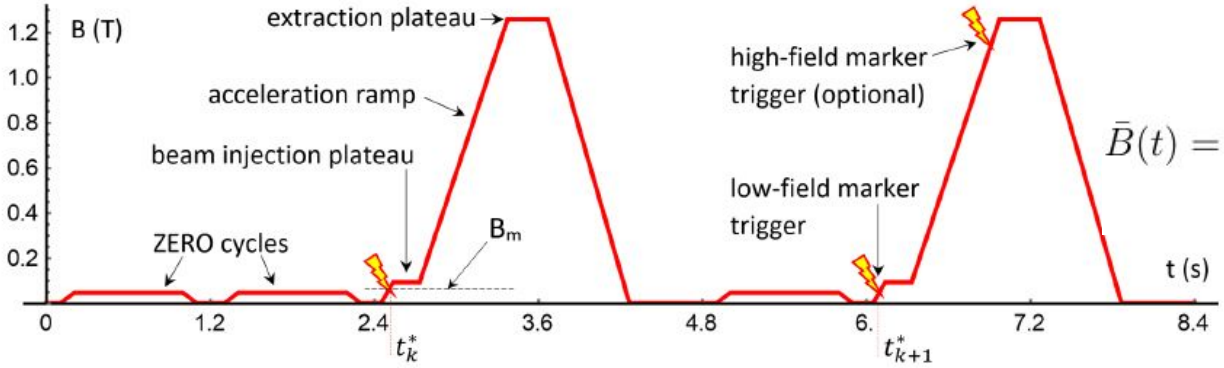

Schematic example of a sequence of magnetic cycles in the Proton Synchrotron

$$V_c = -\frac{d\Phi}{dt}$$

$$\bar{B}(t) = B_m + \Delta\bar{B}(t) = B_m - \frac{1}{A_c}\int_{t_k^*}^{t} V_c(\tau)\, d\tau$$

Approach

- Under certain special circumstances, magnetic field measurement feedback is not the best option. For instance, machine operators may want to replace the measured field temporarily with the simulated one as a beam diagnostic tool:
  - Simulated field: Interpolation of data in a database.
  - Predicted field: real-time prediction for the magnetic field (neural networks).

- Distribution of the measurement and/or simulated/predicted values over a dedicated optic fiber network thanks to the White Rabbit protocol.

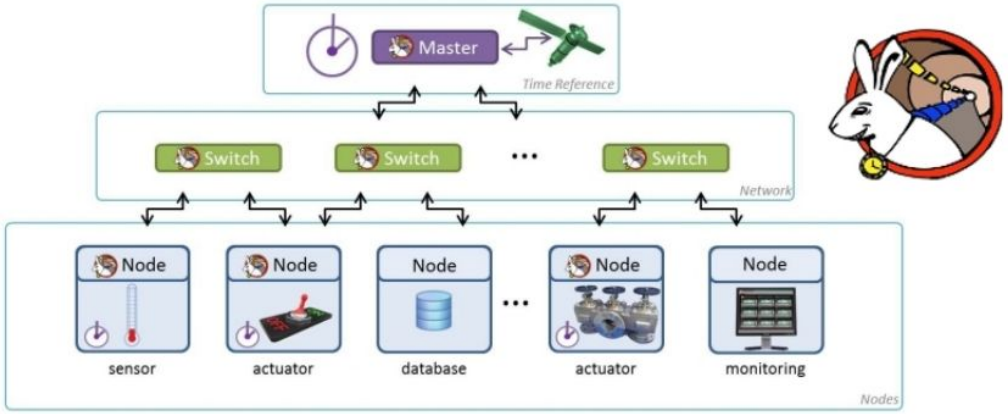

White Rabbit network example

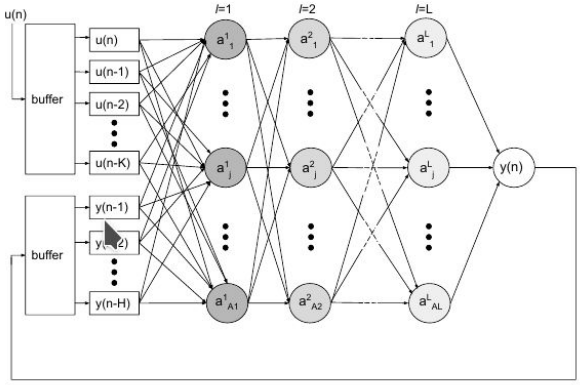

Example of a neural network that can be used to predict the magnetic field in a magnet for particle accelerators

Hardware used

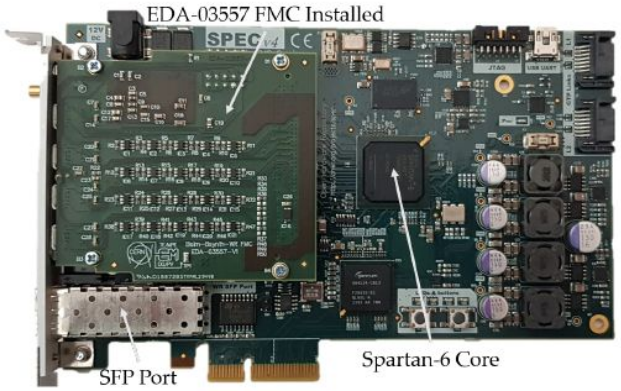

Simple PCI Express carrier (SPEC)

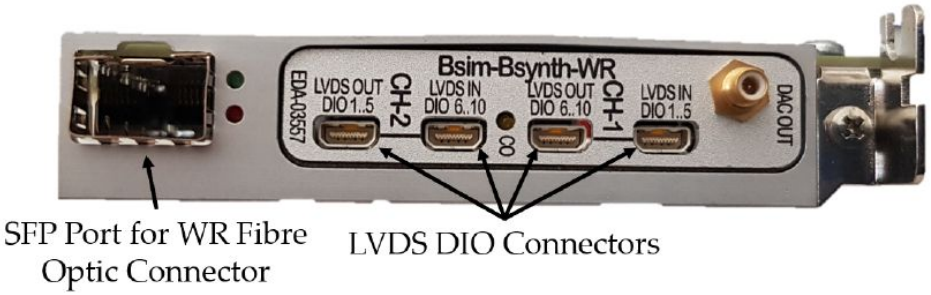

SPEC front view

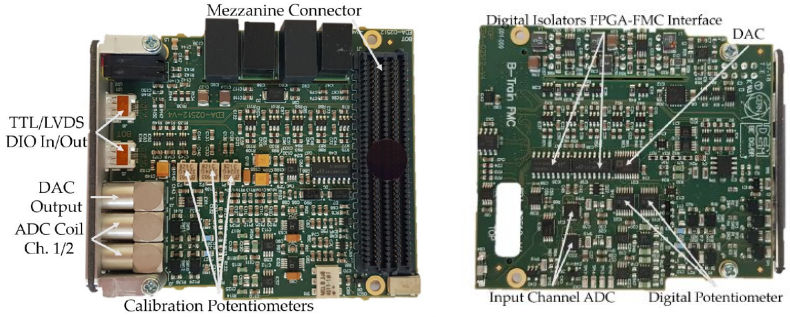

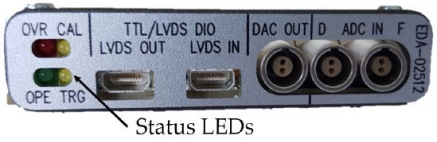

Integrator FMC Board

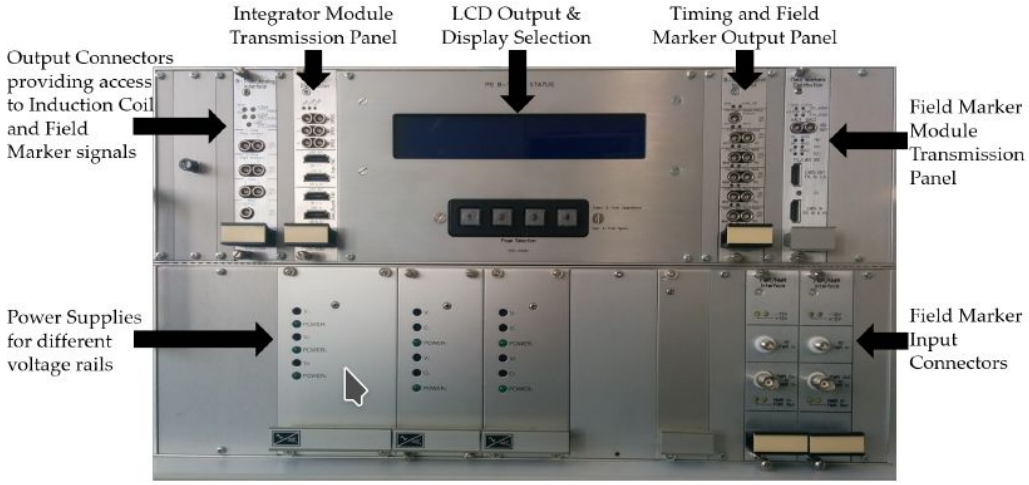

B-Train crate

Development

- The key functions of the novel B-train are implemented by a set of modules based upon off-the-shelf Simple PCIe Carrier (SPEC) hosted in an industrial Front End Computer (FEC).
- Each SPEC card hosts a custom-made FPGA Mezzanine Card (FMC) that implements analogue and digital I/O.
- This architecture allows splitting out the different functions with a fine level of granularity

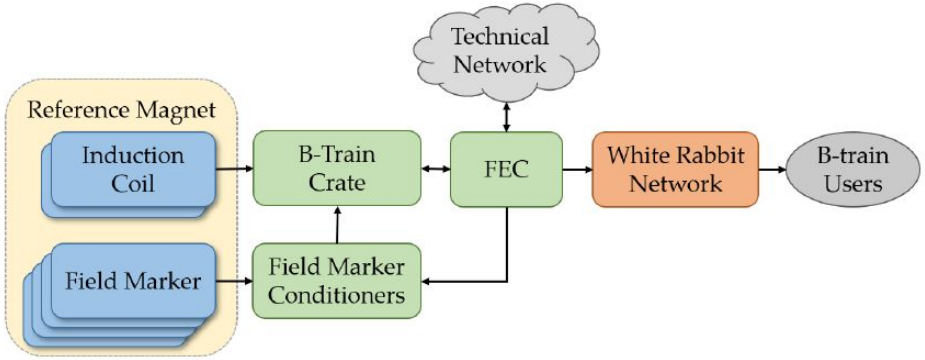

Block diagram of the novel B-Train Project

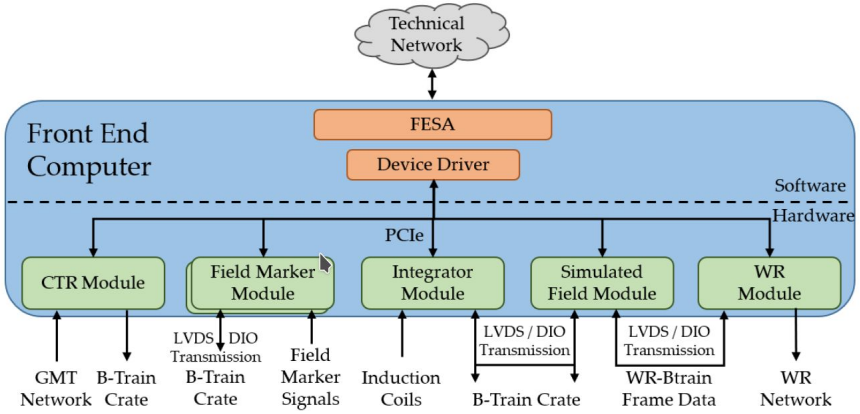

Software hierarchy of the Front end Computer

- Vella Wallbank, J., Amodeo, M., Beaumont, A., Buzio, M., Di Capua, V., Grech, C., ... & Giloteaux, D. (2021). Development of a Real-Time Magnetic Field Measurement System for Synchrotron Control. Electronics, 10(17), 2140.

Analog interface

- A three-way selection switch with a 200 µs settling time for the auto-calibrating.
- An input buffer with a 27 MHz bandwidth and a Rin =2 MΩ impedance.
- A two-stage preamplifier that scales the nominal ±10 V induction coil signal to the ±5 V differential input range of the ADC.
- A digital potentiometer providing a programmable voltage source with 1 mV range and 1 µV resolution, injected between the two attenuation stages and used for fine offset compensation.
- A first-order RC anti-aliasing filter with a 1 MHz cutoff frequency, which gives a nominal 100 ppm maximum error at the upper end of the 100 Hz signal bandwidth.

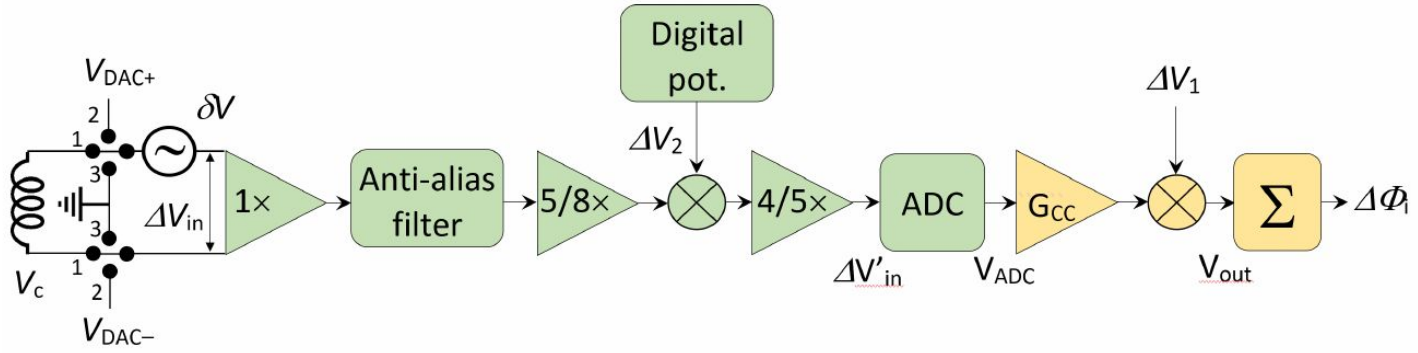

Schematic flowchart of the integrator, including offset and gain correction. The green blocks denote analogue processing steps, while the yellow ones, processing in the digital domain.

Integration Process

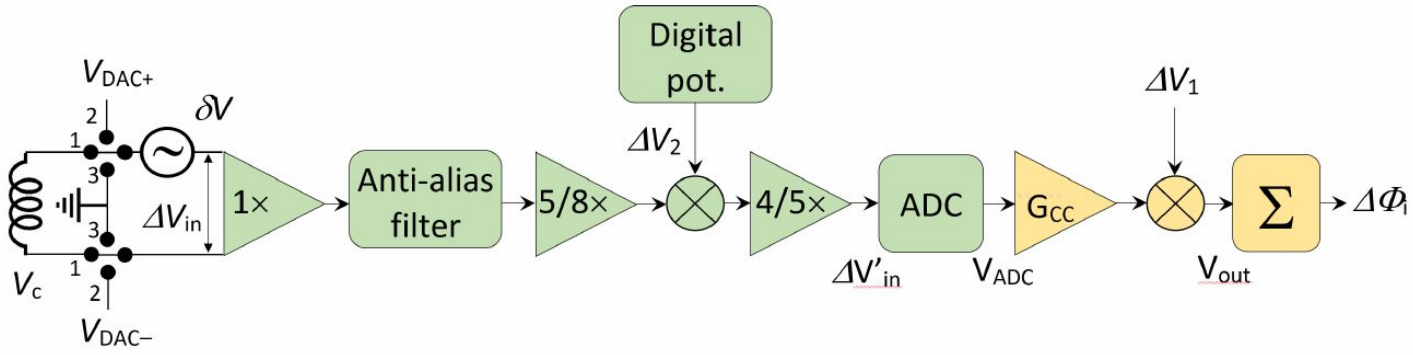

Schematic flowchart of the integrator, including offset and gain correction. The green blocks denote analogue processing steps, while the yellow ones, processing in the digital domain.

$$\Delta V_{\mathrm{in}} = V_{\mathrm{c}} + \delta V \qquad \Delta V'_{\mathrm{in}} = 0.8\,(0.625\Delta V_{\mathrm{in}} + \Delta V_2) = \frac{1}{2}\Delta V_{\mathrm{in}} + \frac{4}{5}\Delta V_2$$

$$V_{\mathrm{out}} = G_{\mathrm{cc}} V_{\mathrm{ADC}} + \Delta V_1 \qquad \Delta\Phi_i = \tau_{\mathrm{s}} \sum_{j=i_k^*}^{i} V_{\mathrm{out},j} \qquad \bar{B}_i = \gamma\left(B_{\mathrm{m}} - \alpha\frac{\Delta\Phi_i}{A_{\mathrm{c}}}\right)$$

Field simulation

- The image of each cycle is stored in the LSA as a two-column vector table, where the first column represents time and the second, in general, the magnetic field. One exception to this rule is provided by the AD, where the LSA image contains the magnet excitation current waveform, and the B-train software must apply a given analytical relationship to derive the magnetic field.

- The vector cycle representation is very compact and a finer resolution is generally required at high field.

- The table of vectors is interpolated to the desired resolution (by default, 4 µs) in real-time in the FPGA, using Bresenham's line algorithm.

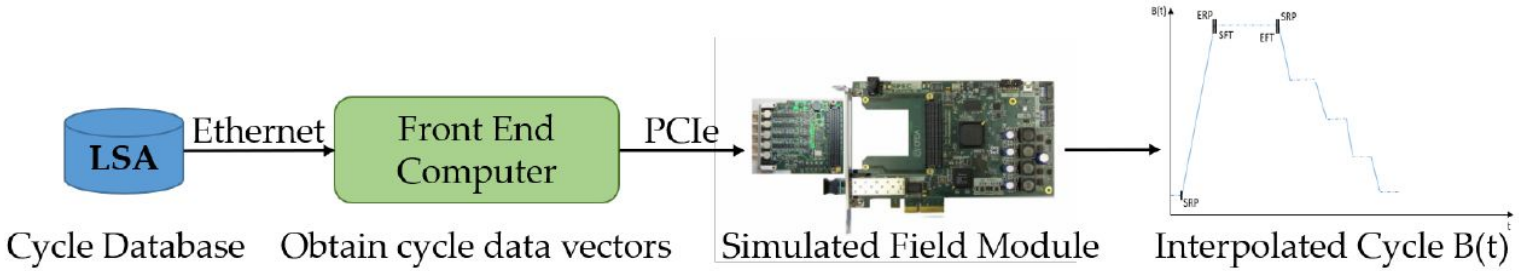

Schematic flowchart of the field simulation.

Field prediction

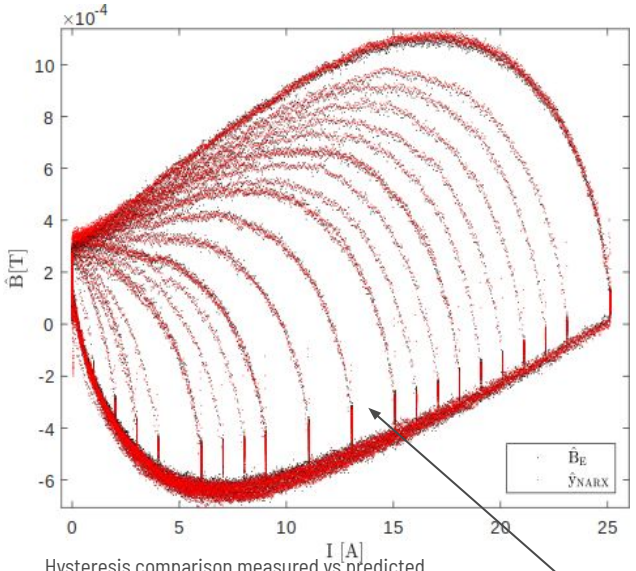

Hysteresis comparison measured vs predicted

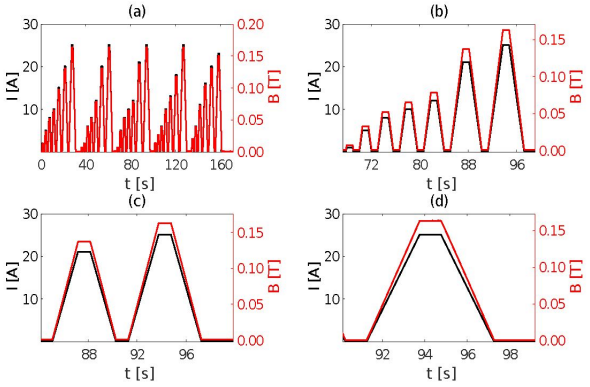

Train and test dataset

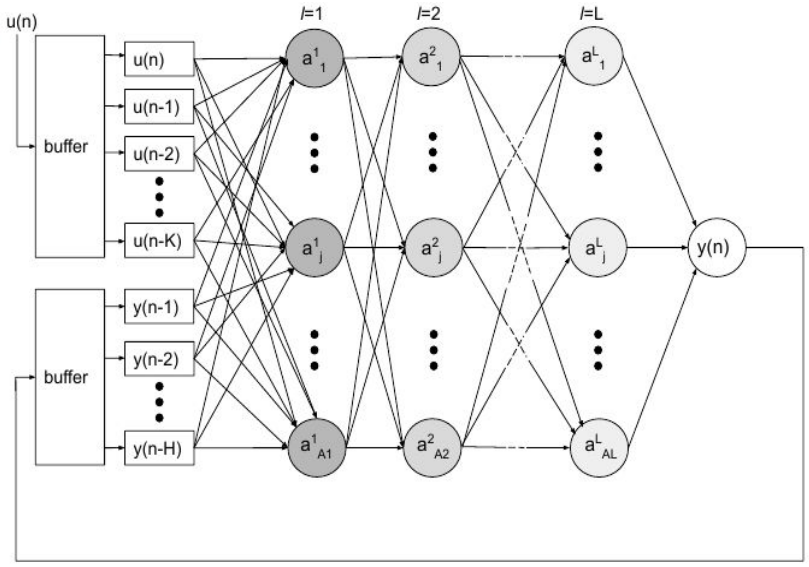

NARX network Layout

20 ppm prediction accuracy

- A NARX neural network to predict hysteresis in iron dominated magnets.
- Feedback from the previous predictions.

- Algorithm developed in Matlab, ported in Python to be used in the CCC for the SPS

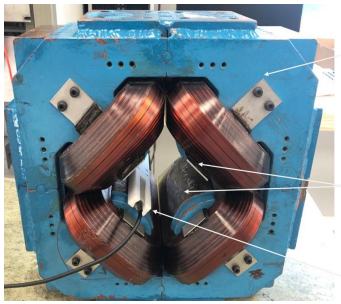

Correction quadrupole used as a case study

- Amodeo, M., Arpaia, P., Buzio, M., Di Capua, V., & Donnarumma, F. (2021). Hysteresis Modeling in Iron-Dominated Magnets Based on a Multi-Layered NARX Neural Network Approach. International journal of neural systems, 31(09), 2150033.

Tool for diagnostic and characterization

- Monitoring the WR payloads at full speed is an essential part of the commissioning and operation phases.
- Noise and glitches in the field measurement can affect destructively the beams and require full bandwidth to be evaluated correctly.

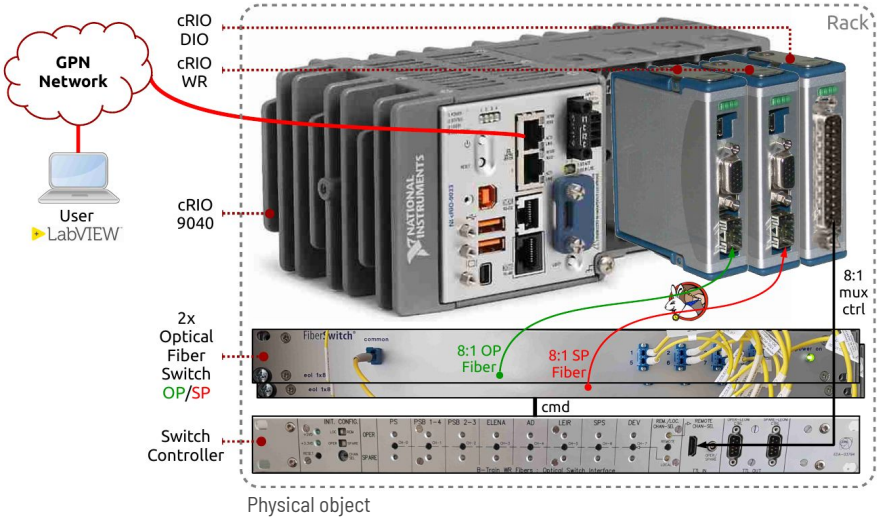

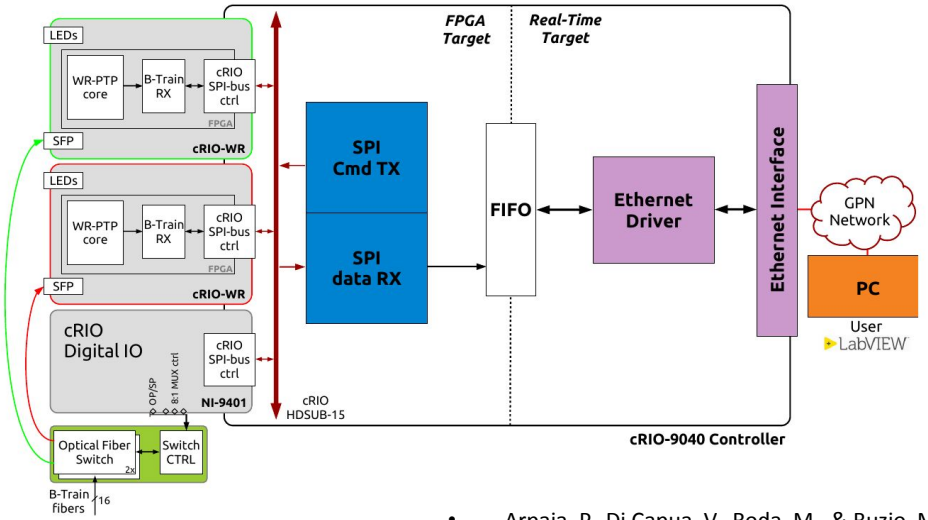

Block diagram.

- Arpaia, P., Di Capua, V., Roda, M., & Buzio, M. (2019). Real-Time Magnetic Measurement Monitoring under cRIO-LabVIEW Based Platform (No. 1335). EasyChair.

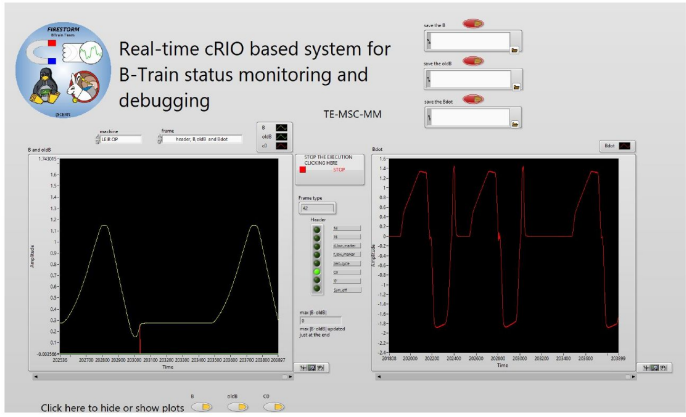

Labview user interface.

System DC characterization

- The accuracy of the voltage measurement, including the in-built gain and the coarse offset corrections, was determined by comparing the known input with the values of VADC and Vout taken from the internal FPGA registers.
- The accuracy of the flux measurement was determined by integrating a constant input voltage Vin in the range ±Vref over a precisely set duration of Δt = 1 s, taking a zero integration constant, and comparing the output $\Delta\Phi$, as read from the FPGA register, to the expected value VinΔt.

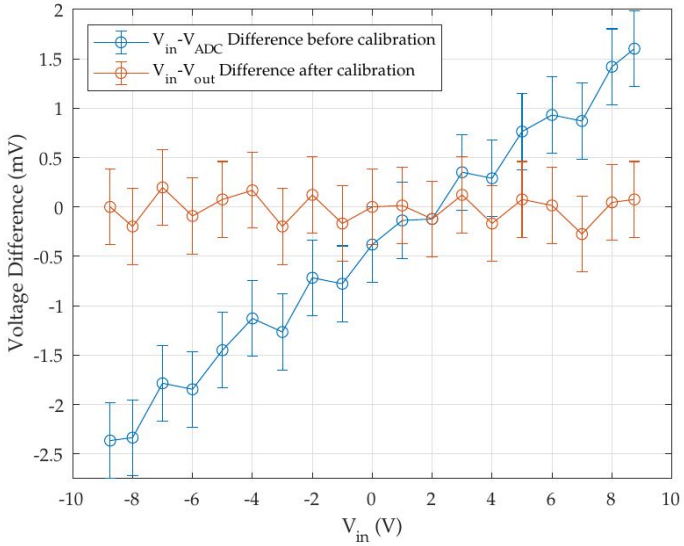

Sensors positioning in the ELENA reference magnet

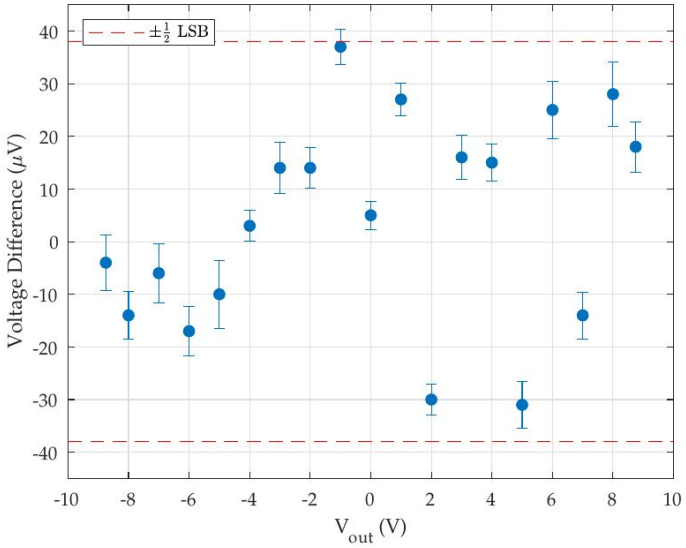

Mean and standard deviation of $\Delta\Phi/\Delta t$ -Vin over the full input dynamic range.

System dynamic characterization

- The gain response was measured as a function of frequency by injecting into the integrator for 1 s sine waves of varying amplitude i.e. 1, 5 and 10 Vpp, and then retrieving the $\Delta\Phi(t)$ waveform from the White Rabbit stream at the receiver's end

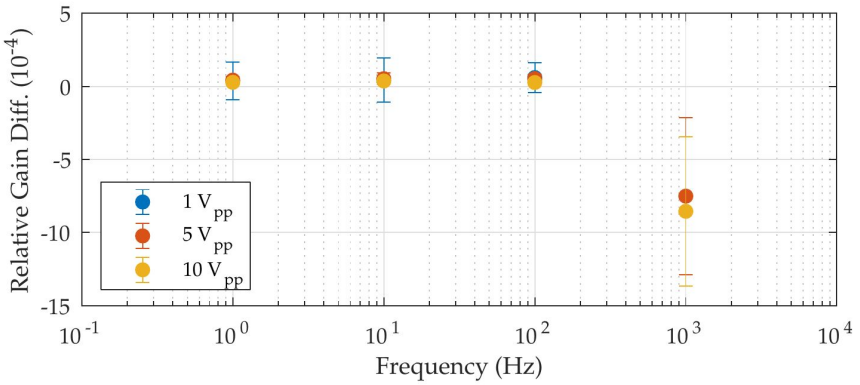

Dynamic gain response.

- The propagation of a step change in the input along the chain was analyzed, to determine the contribution of each processing and transmission stage.

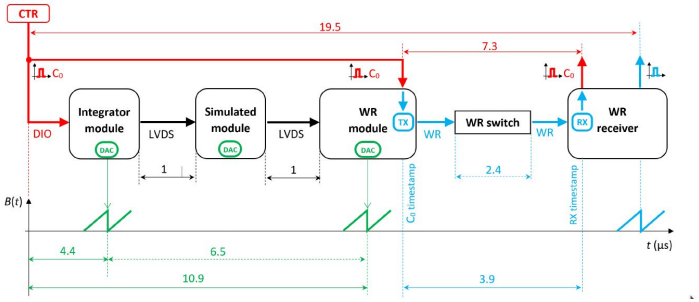

Latency test.

	Input to Output at 250 kHz (µs)	Transmission at 250 kHz (µs)	Input to Output at 100 kHz (µs)	Transmission at 100 kHz (µs)
Average	19.5	7.3	22.6	8.3
Minimum	15.6	4.9	15.7	5.0
Maximum	23.8	9.9	29.7	11.7
σ	2.3	1.2	3.6	1.9

Overall system latency

Drift-free integrators and data fusion

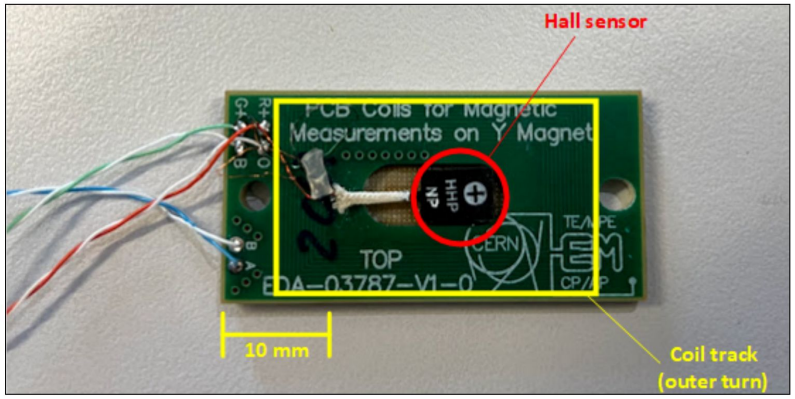

Combined field sensors.

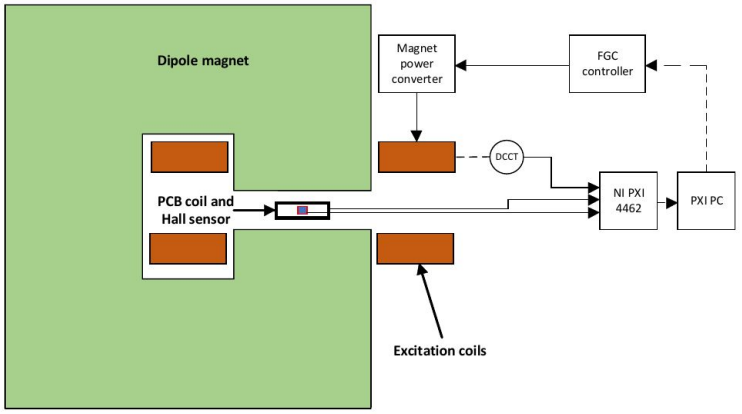

Measurement layout.

	Ramp rate			
	3.2 A/s	32 A/s	100 A/s	Unit
Uncorrected integral	112.14	119.98	59.90	ppm/s
FFA1 - Initial zero-reading average	59.25	8.03	53.02	ppm/s
FFA2 - Online updating algorithm	55.47	5.05	2.95	ppm/s
CS1 - Kalman filter with Hall probe	0.03	0.04	0.03	ppm/s
CS2 - Kalman filter with excitation current	0.02	0.03	0.08	ppm/s

Achieved performance

- Arpaia, P., Buzio, M., Di Capua, V., Grassini, S., Parvis, M., & Pentella, M. (2022). Drift-Free Integration in Inductive Magnetic Field Measurements Achieved by Kalman Filtering. Sensors, 22(1), 182.

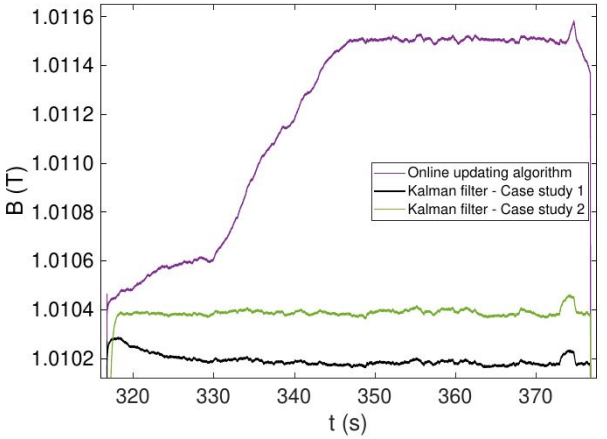

Comparison of the tested techniques.

Side activity 1/2 Metabolic Predictor

- **Problem:**

Type 1 diabetes (T1D) is an autoimmune chronic condition. Even with hybrid-closed loop systems the main challenge for them remains to regulate the insulin delivery at meal time. Commercial algorithms considered exclusively carbohydrates as meal intake, omitting other nutritional factors that are relevant too.

- An machine learning architecture to predict blood glucose up to 180 minutes after meals and to take into account other nutritional factors too such as fats and proteins was developed.

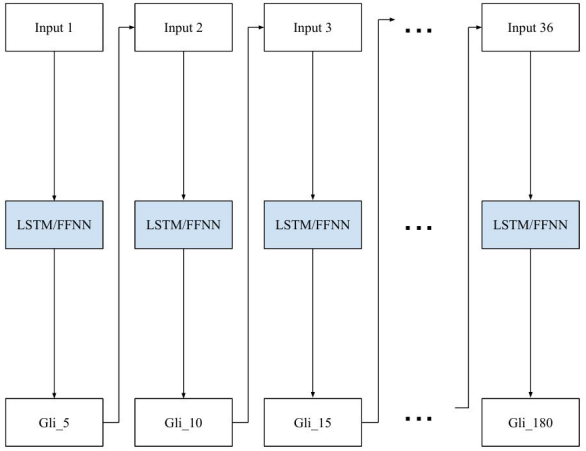

Architecture developed.

ANNs	RMSE (*mean* ± *SD mg/dl*)	RMSPE (*mean* ± *SD %*)
FFNNs	5.89 ± 5.41	4.72 ± 1.65
LSTMs	45.11 ± 58.28	20.42 ± 17.71

Performance achieved.

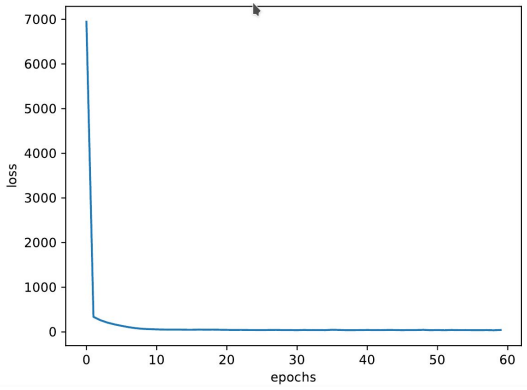

Loss function.

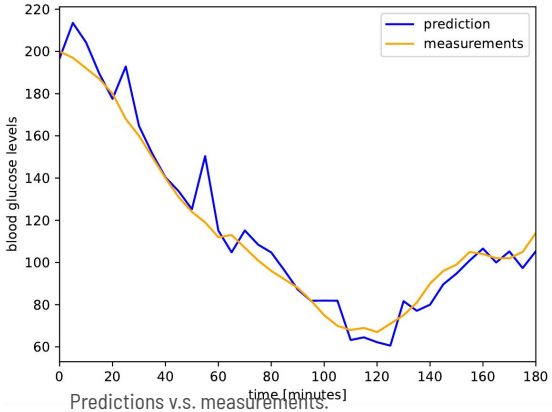

Predictions v.s. measurements.

- P. Arpaia, G. Annuzzi, E. De Benedetto, V. Di Capua, R. Prevete, E. Vallefuoco (2021). "Full nutritional factor Neural network based Metabolic predictors", Nature scientific reports, (submitted).

Side activity 2/2 Vascularization quality

- **Problem:**
  - Indocyanine green (ICG) is a molecule that becomes fluorescent when illuminated with infrared light. ICG has been largely used in the surgical field to estimate the vascularization quality in laparoscopic surgery Currently, the fluorescence brightness of ICG is evaluated only qualitatively and subjectively by the surgeon, based on their experience.
- A ML-based system capable to identify if an intestinal sector is adequately vascularized after an injection of ICG was developed.

Proposed architecture.

Network	Kernel	Neurons L1	Neurons L2	Activation function	Accuracy (%)
SVM	Linear	-	-	-	54.5 ± 15.6
SVM	Gaussian	-	-	-	45.4 ± 23.8
FFNN	-	**20**	-	**ReLU**	**99.9 ± 1.9**
FFNN	-	80	-	Tanh	54.1 ± 28.6
FFNN	-	100	-	Sigmoid	86.0 ± 7.6
FFNN	-	90	90	ReLU	85.2 ± 15.0
FFNN	-	50	50	Tanh	69.9 ± 22.9
FFNN	-	90	70	Sigmoid	68.5 ± 24.2

Classification performance.

- P.Arpaia, U.Baracale, F.Corcione, E. De Benedetto, A. Di Bernardo, V. Di Capua, R. Prevete (2021). “Machine Learning-based assessment of the vascularization quality in laparoscopic colorectal surgery”, Nature scientific reports, (submitted).

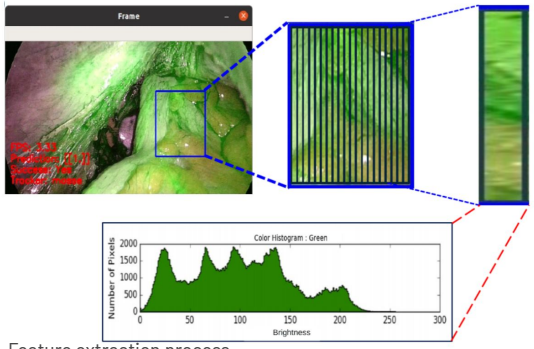

Feature extraction process

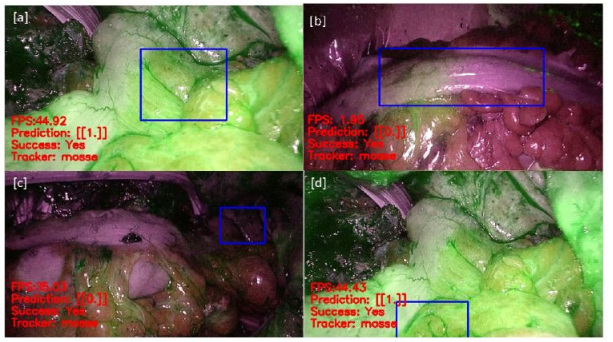

Examples of the algorithm at work.

Production

Journal papers:

- Arpaia, P., Buzio, M., Di Capua, V., Grassini, S., Parvis, M., & Pentella, M. (2022). Drift-Free Integration in Inductive Magnetic Field Measurements Achieved by Kalman Filtering. Sensors, 22(1), 182.
- Amodeo, M., Arpaia, P., Buzio, M., Di Capua, V., & Donnarumma, F. (2021). Hysteresis Modeling in Iron-Dominated Magnets Based on a Multi-Layered NARX Neural Network Approach. International journal of neural systems, 31(09), 2150033.
- Vella Wallbank, J., Amodeo, M., Beaumont, A., Buzio, M., Di Capua, V., Grech, C., ... & Giloteaux, D. (2021). Development of a Real-Time Magnetic Field Measurement System for Synchrotron Control. Electronics, 10(17), 2140.
- Grech, Christian, et al. "Error characterization and calibration of real-time magnetic field measurement systems." Nuclear Instruments and Methods in Physics Research Section A: Accelerators, Spectrometers, Detectors and Associated Equipment 990 (2021): 164979.
- Arpaia, P., Di Capua, V., Roda, M., & Buzio, M. (2019). Real-Time Magnetic Measurement Monitoring under cRIO-LabVIEW Based Platform (No. 1335). EasyChair.
- P.Arpaia, U.Baracale, F.Corcione, E. De Benedetto, A. Di Bernardo, V. Di Capua, R. Prevete (2021). “Machine Learning-based assessment of the vascularization quality in laparoscopic colorectal surgery”, Nature scientific reports, (submitted).
- P. Arpaia, G. Annuzzi, E. De Benedetto, V. Di Capua, R. Prevete, E. Vallefuoco (2021). “Full nutritional factor Neural network based Metabolic predictors”, Nature scientific reports, (submitted).

Production

Conference papers:

- Velotti, F. M., Bartosik, H., Buzio, M., Cornelis, K., Di Capua, V., Fraser, M. A., ... & Kain, V. (2019, June). Characterisation of SPS Slow Extraction Spill Quality Degradation. In 10th Int. Particle Accelerator Conf.(IPAC'19), Melbourne, Australia, 19-24 May 2019 (pp. 2403-2405). JACOW Publishing, Geneva, Switzerland.

- P. Arpaia, G. Annuzzi, E. De Benedetto, V.Di Capua, R. Prevete, E. Vallefuoco (2021). “Neural Network-Based Prediction and Monitoring of Blood Glucose Response to Nutritional Factors in Type-1 Diabetes”, I2MTC,(submitted).

Thank you for your attention

Backup

- Field marker

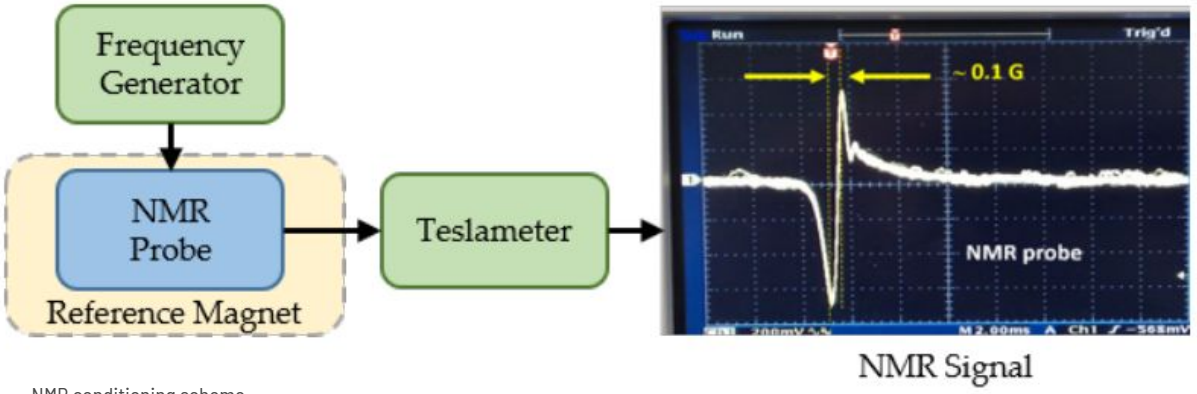

NMR conditioning scheme.

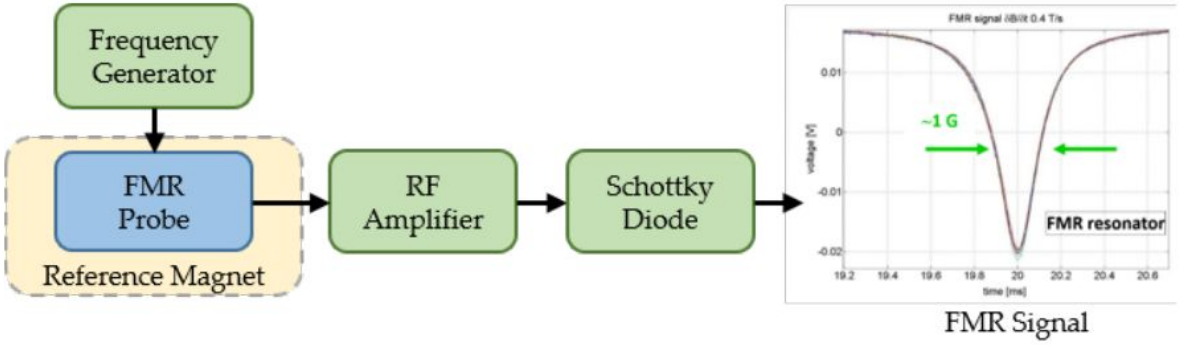

FMR conditioning scheme.

Backup

- Peak detection algorithm.

$$j = min(i) : \begin{cases} t_1 \leq t_i \leq t_2 \\ |V_{\mathrm{m},i}| \geq \overline{V} \\ sign(\dot{V}_{\mathrm{m},i}) \neq sign(\dot{V}_{\mathrm{m},i-1}) \end{cases}$$

i is the running index of the waveform samples; [t1, t2] is a predefined gating window, typically 20 ms long, that prevents spurious triggers to happen too far from the expected time during a cycle; V̇m is the time derivative of the sensor output, calculated with a seven-point finite-difference scheme; and V signed represents a voltage threshold, set independently for each system above the residual noise level after filtering.

Backup

- White Rabbit frame composition.

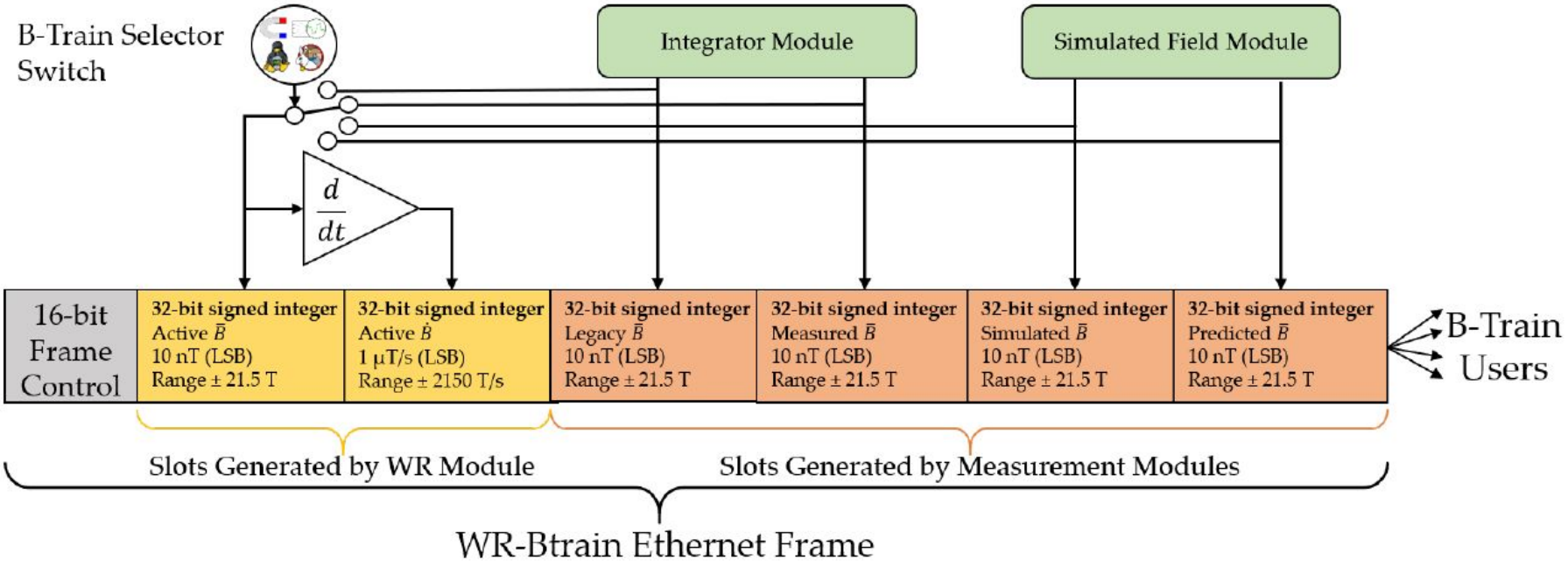

Backup

- Estimated integrator drift.

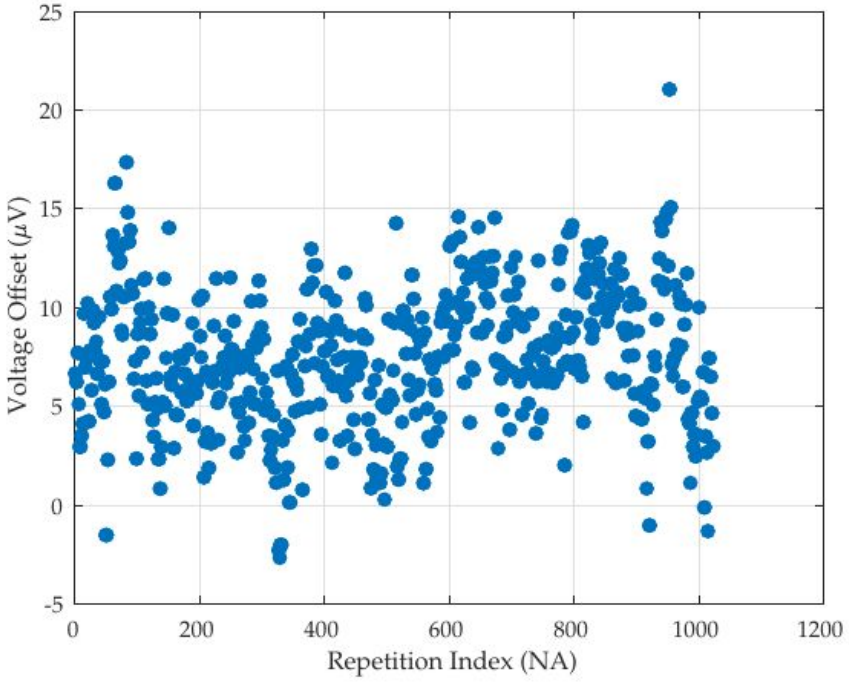

(A) Linearly estimated offset over 1 second

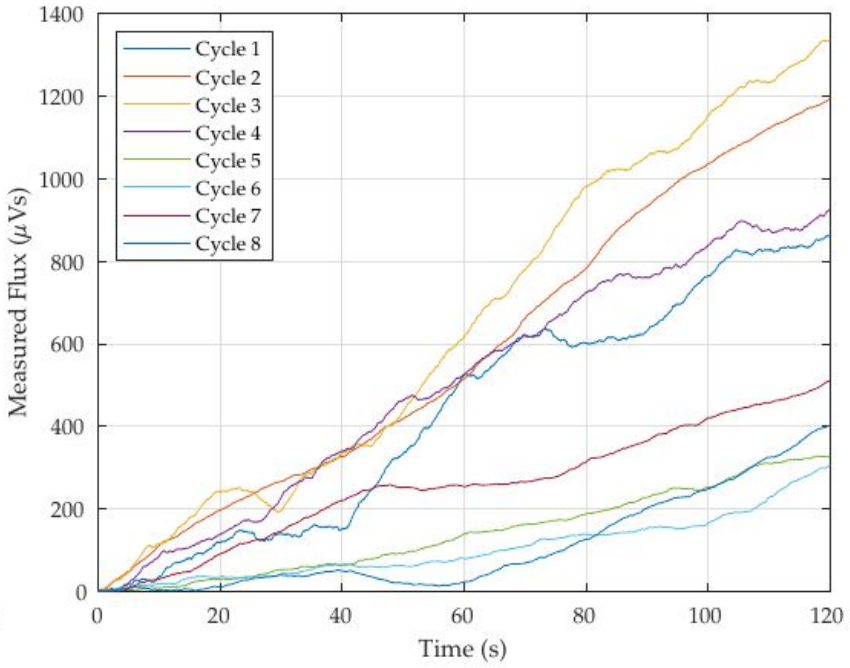

(B) Integrator drift over 120 second

Backup

- Latency impact of the switch

	Input to Output at 250 kHz (µs)	**Transmission at 250 kHz (µs)**	**Input to Output at 100 kHz (µs)**	**Transmission at 100 kHz (µs)**
Average	19.5	7.3	22.6	8.3
Minimum	15.6	4.9	15.7	5.0
Maximum	23.8	9.9	29.7	11.7
σ	2.3	1.2	3.6	1.9

TABLE 10.2: Delay across the White Rabbit network @ 250 $kfps$

	Without Switch (µs)	**With Switch (µs)**
Average	1.53	3.93
Minimum	1.52	3.86
Maximum	4.32	7.2
σ	0.13	0.13

TABLE 10.3: Internal FEC propagation time @ 250 $kfps$

	C_0 to Integrator DAC (µs)	**C_0 to WR DAC (µs)**
Average	4.4	10.9
Minimum	1.8	8.4
Maximum	6.8	13.3
σ	1.2	1.7

Backup

- NARX Network

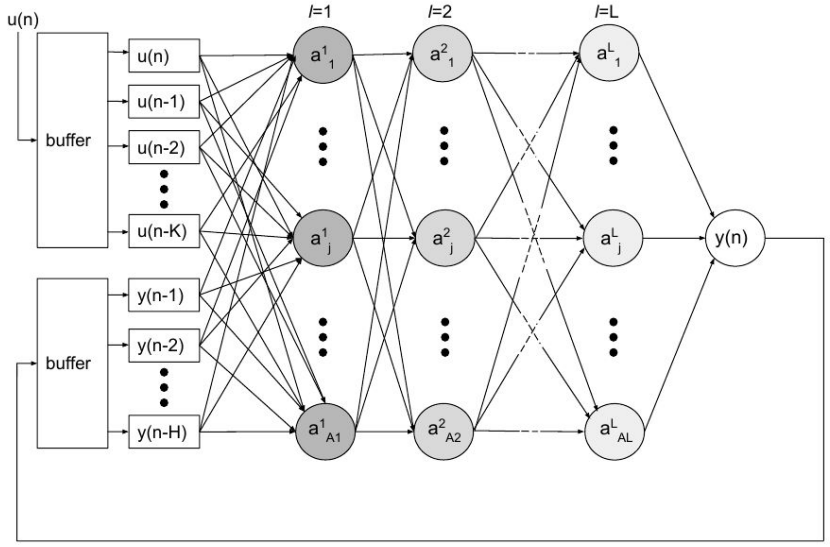

$$a_j^1(n) = \phi^{A_1}\left(\sum_{h=1}^{H} W_{jh}^O y(n-h) + \sum_{k=0}^{K} W_{jk}^I u(n-k)\right)$$

$$a_j^l(n) = \phi^{A_l}\left(\sum_{i=0}^{A_l} W_{ji}^l a_i^{l-1}(n)\right)$$

$$y(n) = \sum_{i=0}^{A_{L-1}} W_i^E a_i^L(n)$$

- φ_{A1} is the activation function of the neurons of the layer.
- W are the weight of the interconnections.

Backup

- Networks performance.

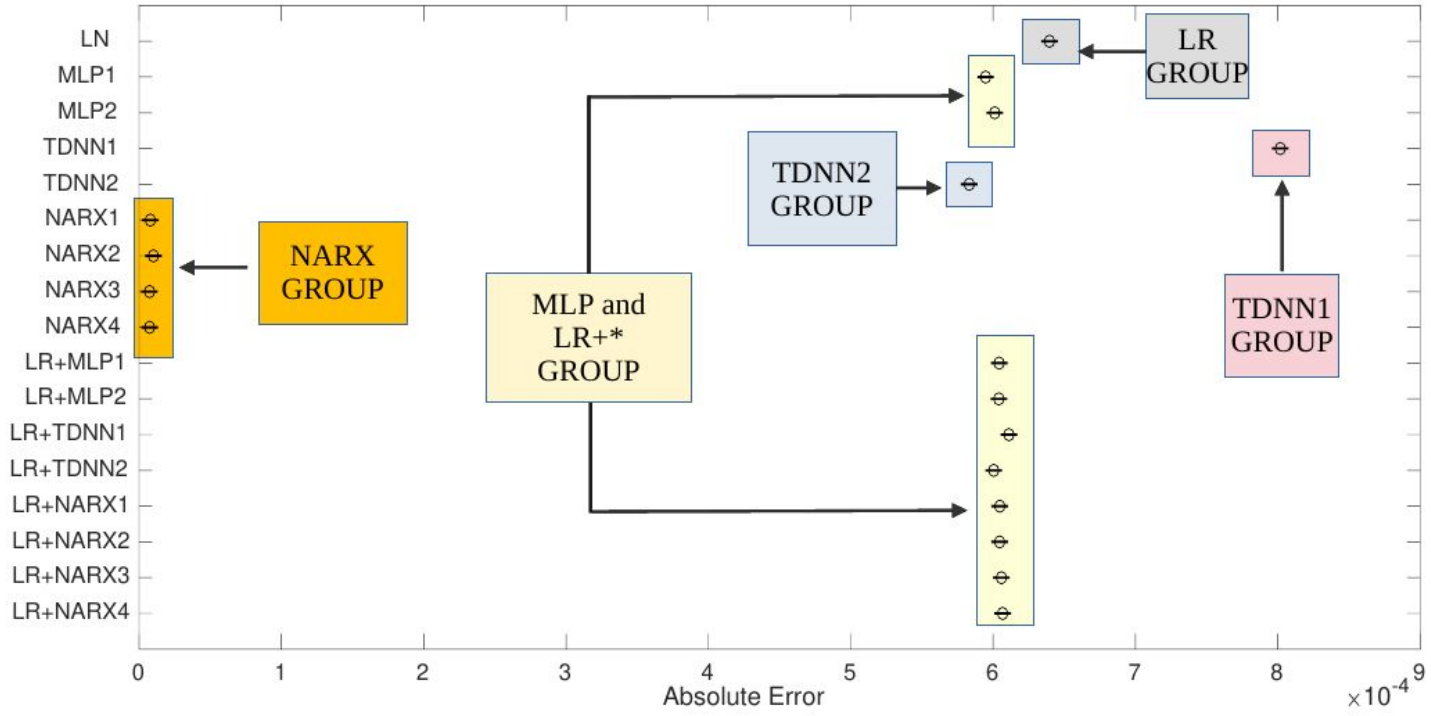

ANOVA results on Absolute Errors computed for the competing models on Dataset DE . The horizontal lines are the 95 % confidence interval for each model. Five groups are highlighted: LR group (gray), MLP group and LR+* group (yellow), TDNN1 (pink), TDNN2 (in blue) and the NARX group (orange)

Backup

- Networks performance.

Architecture	Test Dataset	Hyper--parameters	RMSE [T]	NMRSE (%)	MAE [T]	MPE (%)
Linear Regression		G, B_0	$9.07 \cdot 10^{-04}$	$5.67 \cdot 10^{-01}$	$2.60 \cdot 10^{-03}$	1.61
MLP1	$\bar{D}_{\mathrm{E}}$	$\tilde{\theta}_{MLP1}$	$8.70 \cdot 10^{-04}$	$5.44 \cdot 10^{-01}$	$2.60 \cdot 10^{-03}$	1.64
MLP2	$\bar{D}_{\mathrm{E}}$	$\tilde{\theta}_{MLP2}$	$8.83 \cdot 10^{-04}$	$5.52 \cdot 10^{-01}$	$2.50 \cdot 10^{-03}$	1.55
TDNN1	$\bar{D}_{\mathrm{E}}$	$\tilde{\theta}_{TDNN1}$	$1.10 \cdot 10^{-03}$	$6.66 \cdot 10^{-01}$	$2.70 \cdot 10^{-03}$	1.67
TDNN2	$\bar{D}_{\mathrm{E}}$	$\tilde{\theta}_{TDNN2}$	$8.52 \cdot 10^{-04}$	$5.32 \cdot 10^{-01}$	$2.50 \cdot 10^{-03}$	1.56
NARX1	$\bar{D}_{\mathrm{E}}$	$\tilde{\theta}_{NARX1}$	$9.92 \cdot 10^{-06}$	$6.20 \cdot 10^{-03}$	$4.63 \cdot 10^{-05}$	$2.89 \cdot 10^{-02}$
NARX2	$\bar{D}_{\mathrm{E}}$	$\tilde{\theta}_{NARX2}$	$1.27 \cdot 10^{-05}$	$8.00 \cdot 10^{-03}$	$6.90 \cdot 10^{-05}$	$4.31 \cdot 10^{-02}$
NARX3	$\bar{D}_{\mathrm{E}}$	$\tilde{\theta}_{NARX3}$	$9.22 \cdot 10^{-06}$	$5.80 \cdot 10^{-03}$	$3.98 \cdot 10^{-05}$	$2.49 \cdot 10^{-02}$
NARX4	$\bar{D}_{\mathrm{E}}$	$\tilde{\theta}_{NARX4}$	$9.28 \cdot 10^{-06}$	$5.80 \cdot 10^{-03}$	$4.06 \cdot 10^{-05}$	$2.54 \cdot 10^{-02}$
LR+MLP1	$\bar{D}_{\mathrm{E}}$	G, B_0, $\tilde{\theta}_{MLP1}$	$8.00 \cdot 10^{-04}$	$5.00 \cdot 10^{-01}$	$1.90 \cdot 10^{-03}$	1.16
LR+MLP2	$\bar{D}_{\mathrm{E}}$	G, B_0, $\tilde{\theta}_{MLP2}$	$8.00 \cdot 10^{-04}$	$5.00 \cdot 10^{-01}$	$1.90 \cdot 10^{-03}$	1.17
LR+TDNN1	$\bar{D}_{\mathrm{E}}$	G, B_0, $\tilde{\theta}_{TDNN1}$	$8.05 \cdot 10^{-04}$	$5.03 \cdot 10^{-01}$	$1.90 \cdot 10^{-03}$	1.18
LR+TDNN2	$\bar{D}_{\mathrm{E}}$	G, B_0, $\tilde{\theta}_{TDNN2}$	$7.97 \cdot 10^{-04}$	$4.98 \cdot 10^{-01}$	$1.90 \cdot 10^{-03}$	1.18
LR+NARX1	$\bar{D}_{\mathrm{E}}$	G, B_0, $\tilde{\theta}_{NARX1}$	$7.98 \cdot 10^{-04}$	$4.99 \cdot 10^{-01}$	$1.90 \cdot 10^{-03}$	1.17
LR+NARX2	$\bar{D}_{\mathrm{E}}$	G, B_0, $\tilde{\theta}_{NARX2}$	$7.98 \cdot 10^{-04}$	$4.99 \cdot 10^{-01}$	$1.90 \cdot 10^{-03}$	1.17
LR+NARX3	$\bar{D}_{\mathrm{E}}$	G, B_0, $\tilde{\theta}_{NARX3}$	$7.99 \cdot 10^{-04}$	$5.00 \cdot 10^{-01}$	$1.90 \cdot 10^{-03}$	1.17
LR+NARX4	$\bar{D}_{\mathrm{E}}$	G, B_0, $\tilde{\theta}_{NARX4}$	$8.00 \cdot 10^{-04}$	$5.00 \cdot 10^{-01}$	$1.90 \cdot 10^{-03}$	1.17

Backup

- Networks performance in literature.

Architecture	Metric	Value
Deep Neural Network (MLP with two hidden layers)	Root Mean Square Error	0.13 %
Preisach + Feed-forward neural network (one hidden layer)	Maximum Absolute Error	13 %
Preisach	Relative Error	0.2 %
Preisach + Recurrent Neural Network	Normalized Root Mean Square Error	0.7%
Neural Network	Relative Error	< 8 %
Genetic Algorithm + Neural Network	Mean Square Error	< 5 %

Backup

- drift free integrator with Kalman

$$B(t) = B_0 + \frac{1}{A_c}\int_0^t v(\tau)d\tau \qquad v(t) = v_s(t) + v_o(t) \qquad \hat{\mathbf{P}}_k^- = \mathbf{F}\hat{\mathbf{P}}_{k-1}^+\mathbf{F}^T + \sigma_{w,k}^2$$

$$\hat{\mathbf{P}}_k^+ = (\mathbf{I} - \mathbf{K}_k\mathbf{D})\hat{\mathbf{P}}_k^-$$

$$\mathbf{x}_k = \mathbf{F}\mathbf{x}_{k-1} + \mathbf{C}\mathbf{u}_k + \mathbf{w}_k \qquad \mathbf{z}_k = \mathbf{D}\mathbf{x}_k + \mathbf{q}_k$$

$$\hat{\mathbf{x}}_k^- = \mathbf{F}\hat{\mathbf{x}}_{k-1}^+ + \mathbf{C}\mathbf{u}_k \qquad \hat{\mathbf{x}}_k^+ = \hat{\mathbf{x}}_k^- + \mathbf{K}_k\mathbf{y}$$

$$\mathbf{y} = \mathbf{z}_k - \mathbf{D}\hat{\mathbf{x}}_k^-$$

$$\hat{\mathbf{x}}_k^+ = \hat{\mathbf{x}}_k^- + \mathbf{K}_k\mathbf{y}$$

$$x_k = B_k = B_{k-1} + \frac{1}{A_c}\frac{(v_k + v_{k-1})}{2}T_s$$

$$\mathbf{K}_k = \hat{\mathbf{P}}_k^-\mathbf{D}^T(\sigma_{q,k}^2 + \mathbf{D}\hat{\mathbf{P}}_k^-\mathbf{D}^T)$$

$$\sigma_{w,k}^2 = \frac{T_s^2}{4A_c^2}\left(\frac{\sigma_A^2}{A_c^2}(v_k + v_{k-1})^2 + (\sigma_{v,k}^2 + \sigma_{v,k-1}^2)\right)$$

$$z_k = B_{H,k} = B_k + q_k$$

- K=kalman gain
- x=vector state
- u= input=vk+vk-1
- **P**= covariance matrix
- **C**= input matrix=Ts/2Ac
- **D**= measurement Matrix=1
- **F**= state-transition matrix=1
- **w**= process noise vector
- **q=**measurement noise vector

Backup

- drift free integrator with Kalman Filter uncertainty

	Ramp rate			
	3.2 A/s	**32 A/s**	**100 A/s**	Unit
Uncorrected integral	194.48	104.23	60.34	mT
FFA1 - Initial zero-reading average	100.25	9.38	25.97	mT
FFA2 - Online updating algorithm	37.57	6.53	5.53	mT
CS1 - Kalman filter with Hall probe	65	65	65	μT
CS2 - Kalman filter with excitation current	667	533	482	μT

$$\sigma_{B,k} = \sqrt{P_k} + (B_k - B_k^{CS1})$$

- For CS1 and CS2, for P_k the a posteriori variance estimated by the Kalman filter is used.
- For the uncorrected integral and the two algorithms FFA1 and FFA2, for P_k the a priori variance is used.